

UPCommons

Portal del coneixement obert de la UPC

<http://upcommons.upc.edu/e-prints>

© 2018 IEEE. Personal use of this material is permitted. Permission from IEEE must be obtained for all other uses, in any current or future media, including reprinting/republishing this material for advertising or promotional purposes, creating new collective works, for resale or redistribution to servers or lists, or reuse of any copyrighted component of this work in other works

Aquesta és una còpia de la versió author's final draft de l'article Thermography-based methodology for multifault diagnosis on kinematic chain publicat a IEEE transactions on industrial informatics.

URL d'aquest document a UPCommons E-prints:
<http://hdl.handle.net/2117/127823>

Article publicat / *Published paper:*

Delgado Prieto, M. [et al.]. Thermography-based methodology for multifault diagnosis on kinematic chain. "IEEE transactions on industrial informatics", 1 Desembre 2018, vol. 14, núm. 12, p. 5553-5562.

Thermography based Methodology for Multi-fault Diagnosis on Kinematic Chain

Abstract—The thermographic procedures for condition monitoring of electromechanical systems are undergoing a reformulation, mainly, due to the current affordability of infrared cameras to be incorporated on industrial applications. However, high performing multi-fault data-driven methodologies must be investigated in order to infer reliable condition information from the thermal distribution of the electrical motors, but also, shafts and couplings. To address this issue, a novel thermography based methodology is proposed. First, the infrared capture is processed to obtain a thermographic residual image of the kinematic chain. Second, the thermal distribution of the image's regions of interest are characterized by means of statistical features. Finally, a distributed self-organizing map structure is used to model the nominal thermal distribution to subsequently perform a fault detection and identification. The method provides a reliability quantification of the resulting condition assessment in order to avoid misclassifications and identify the actual fault root-causes. The performance and the effectiveness of the proposed methodology is validated experimentally and compared with the classical maximum temperature gradient procedure.

Index Terms— Condition monitoring; Fault diagnosis; Infrared imaging; Rotating machines; Self-organizing feature maps, industry applications.

I. INTRODUCTION

UNEXPECTED fault conditions may arise during the useful life of electromechanical systems under continuous operation, as is usual in industrial environments. The consequent unscheduled downtimes of the associated processes lead to non-affordable situations that penalize the effectiveness ratio associated to the assets. In this regard, Condition Based Monitoring (CBM), has become accepted by the industrial sector as a strategic aspect to fulfil with the competitiveness requirements. Indeed, a continuous monitoring of kinematic chains, which are formed by electrical machines coupled to rotatory mechanical components, represents one of the main application fields of CBM due to its criticality in multiple industrial processes. In this regard, major fault conditions in induction motor based actuators include bearing defects [1], mechanical unbalances [2, 3], and stator winding insulation [4] among others, with the consequent implication on productivity loss and safety risks. Concerned by this situation a great deal of fault diagnosis methodologies has been presented during the last decade. However, most of these studies are focused on the analysis of specific fault conditions, while the application of CBM schemes to industrial environments presents new challenges that must be addressed; multiple faults conditions may appear, overlapping the expected characteristic patterns among them [5]. In this regard, the diagnosis capabilities of different physical magnitudes such as vibrations, stator currents or

acoustic emissions, among others, are constantly under investigation. Aligned with such trending research topic, new processing procedures for temperature monitoring are proposed in order to enhance the performance of classical diagnosis methods [6-8]. Classically, the thermal analysis has been associated to off-line tests over electrical machines [9], mainly related with defective contacts [10] or insulation failures [11]. The on-line diagnosis applications over electrical machines have been focused on RTD or thermocouple sensors mounted inside the motor during the manufacturing process, usually, over the stator windings or the bearing external cage. However, such approach does not allow the thermal distribution analysis over the electrical machine and, even less, over the rest of the components of the electromechanical system such as shafts, couplings, among others, which limits the significance of the obtained information to identify the root-cause of the malfunction.

As stated in the case stories review presented by D. Lopez-Perez and J. Antonino-Daviu [12], in the last lustrum, the consideration of an infrared camera for thermographic analysis, represents an economically affordable opportunity as useful tool to detect the presence of faults in kinematic chains without interfering with the machine operation. Infrared thermography allows the high precision measurement and visualization of the superficial temperatures of the machine in a noninvasive manner, at a certain distance, and without necessity of any contact. In this regard, different studies have been carried out to establish a relationship between an increasing in temperature with the presence of specific faults within the motor. For instance, M. J. Picazo-Ródenas *et al.* in [13], proposed a fault diagnosis methodology supported by a thermal model of the electrical machine. The thermal differences in front of defective variants of the modelled electrical motor were proven to be effective for diagnosis. Most of the works, however, propose the use of image segmentation procedures to extract some regions of the infrared image [14, 15]. The main advantage of these segmented-based methodologies is that only small parts of the image are analyzed, from where the temperature gradient regarding the nominal condition is extracted. For instance, in the work presented by A. G. Garcia-Ramirez *et al.* in [16], a fault detection methodology based on thermographic images segmentation applied to induction motors was proposed. The methodology includes calibration procedures to improve the estimation of thermal coefficient indexes and, in consequence, the fault diagnosis ratio. These thermographic analysis, although offering good results, are limited to fault detection, where independent temperature thresholds are applied over each segmented component under monitoring. Thus, the presence of only one fault condition may be interpreted as multiple faults over the kinematic chain due to its thermal

affectation, decreasing the diagnosis performance and making difficult the root-cause identification. Some other works, however, propose to extend the diagnosis capabilities towards the fault identification, in which the root-cause of the fault is identified automatically. For instance, the data-driven approach proposed by V. Tung Tran *et al.* in [17], where a diagnosis procedure to identify faults on a shaft attached to an induction motor was performed by means of a pattern recognition scheme. The method, however, does not segment the infrared image in multiple regions. In consequence, although the work performs properly dealing with different sources of faults, the results present a risk of overfitting, since extremely low temperature gradients are considered as characteristic fault patterns.

Indeed, all these approaches exhibit the recent significant interest of the research community in order to study diagnosis procedures capable of increase the condition monitoring capabilities of kinematic chains by means of infrared thermography and, in consequence, posterior combination schemes of infrared data analysis with other physical magnitudes for a diagnosis reliability increase. However, although all the aforementioned methodologies provide proper results in fault detection, the identification of the fault in a multi-fault diagnosis framework is still an open problem. In this regard, there are just several works dealing with the identification of multiple faults, but even less proposing an automatic diagnosis methodology with identification capabilities dealing with the thermal affectation of the faulty part over the rest of the elements of the kinematic chain.

The contribution of this work consists on the proposal of a thermographic data-driven methodology applied to a kinematic chain, composed by an infrared image processing, a segmented feature extraction, and a multi-fault diagnosis scheme. The signal processing stage comprises a thermal image analysis based on the proposed Thermographic Residual Imaging (TRI). Such approach not only allows the posterior extraction of numerical features to characterize the thermal images, but also highlights thermal anomalies from the expected nominal condition. Next, a feature extraction procedure is proposed based on the TRI segmentation to quantify the thermal status of each critical component considered. Finally, the fault detection and identification stage is designed by means of a collaborative structure of Self-Organizing Maps (SOM), which allow the thermal distribution modelling of each mechanical component and, later, the root-cause identification is inferred from the condition diagnosis outcomes and the related reliability indexes. The originality of this work comprises the normalization of the thermal images for temperature deviations enhancement, the estimation of statistical features from the image segmentations in order to characterize the thermal distributions and, also, the modelling of such distributions through topology preservation maps based on neural networks. Thus, resulting in a new information fusion structure for multi-fault diagnosis of electromechanical systems. The proposed method, moreover, allows the data visualization and also the interpretation of the underlying physical phenomenon.

This paper is structured as follows. Section II describes the theoretical aspects of the proposed self-organizing map operation. Section III describes the proposed methodology. The experimental tests to validate the method are discussed in Sections IV. Conclusions are summarized, finally, in Section V.

II. SELF-ORGANIZING MAPS

Dealing with data-driven diagnosis methodologies, the classification stage is commonly faced by means of the compression of the available feature set in order to enhance specific data distribution characteristics; as the variance by means of principal components analysis, or the separation among different conditions by means of linear discriminant analysis. Later, patterns learning algorithms are applied for a posterior recognition of similarities during a new measurement assessment. However, the criticality of this stage and the limitation of some feature reduction techniques has been pointed out by different studies, mainly, dealing with large and disconnected data sets, because they seek for a global structure of the data [18]. Concerning with this problem, manifold learning methods has been applied in the last years [19]. Among them, the self-organizing map is the most used, which is based on developing a neural network grid to preserve most of the original distances between the feature vectors in the original data space.

The self-organizing map learning rule corresponds to a neural network grid trying to preserve the topological properties of an input space. The output space is predefined as a regular grid. Each neuron of the SOM grid represents a Matching Unit, MU. For each neuron, n_i , a D -dimensional weight vector wn_i is defined. The weights represent the coordinates of the neurons in the input space, that is, the number of features. Thus, the mapping is performed by assigning each input data point, din_j , to one of these neurons, namely the one whose weight vector is closest to the point, which is called the Best Matching Unit (BMU). The position vector of each data point in the output space, $dout_j$, is, then, given by the grid position of the corresponding BMU. The used error function corresponds to (1).

$$E_{SOM} = \sum_i \sum_{din_j \in n_i} (wn_i - dout_j)^2 \quad (1)$$

The E_{SOM} expresses the average squared distance from a data point to its representative BMU. The minimization of the E_{SOM} represents the objective of the training, and is performed with respect to the weight vectors wn_i . For each iteration, l , the gradient descent approach leads, classically, to the updating rule (2) based on a learning rate, α .

$$wn_i^{(l+1)} = wn_i^{(l)} - \alpha^{(l)} (\nabla E_{SOM}^{(l)})_i \quad (2)$$

During the training, the $\alpha^{(l)}$ is decreased monotonically, then, preserving the local topology from each neuron unit. Classically, the performance of SOM is evaluated by the average quantization error, E_q . The E_q means the distance from each data vector to its BMU, that is, the local topology mean error.

III. METHODOLOGY

The difference among temperature values measured from different condition in specific components in a kinematic chain represents a qualitative infrared analysis approach widely applied in many industrial applications [20]. It must be considered that, dealing with industrial applications, the temperature measurement during the thermal steady-state regime of the machine is critical. Although the thermal effects exhibit often a low inertia, the inspection during thermal transients would require additional speed and torque characterization procedures. In fact, according to the NETA Standard [21], different recommended maintenance actions are given regarding the value of the temperature difference among the similar components during thermal steady-states, the ΔT criterion. Thus, a ΔT between 1-3 °C implies a possible deficiency where additional investigation is recommended, a ΔT between 4-15 °C indicates probable deficiency, where a repair is recommended, and a ΔT over 15 °C shows a major event, where an immediate reparation is recommended.

Although most of condition-based monitoring schemes are based on the ΔT criterion, it is a common limitation of the proposed methods the consideration of that, *a priori*, no additional fault conditions will take place beyond the considered ones. However, in industrial applications, information regarding faulty conditions is commonly not accessible; just the nominal/healthy condition is measurable. Therefore, the proposed methodologies should offer enough capabilities to detect, identify and incorporate additional conditions throughout the asset useful life. That is, it is expected the detection of a fault presence, its root-cause identification, but also, the recognition of deviations from the characterized condition patterns.

In the proposed methodology, such challenges are considered by means of a four stages condition-monitoring scheme as shown in Fig. 1.

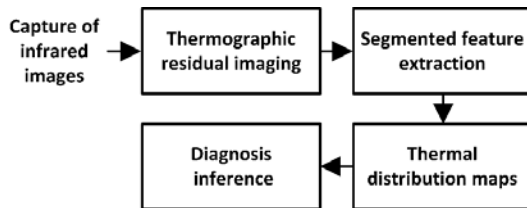


Fig. 1. Thermographic data-driven methodology composed by four main stages.

First, the enhancement of significant thermal deviations from the kinematic chain is performed through the processing of the infrared captures. The resulting thermographic residual images highlight the thermal differences in comparison to the nominal thermal conditions. Second, the feature extraction of such residual thermal distribution for each region of interest follows. That is, each mechanical component of interest is segmented from the image and numerically characterized. Third, the thermal characterization of each considered region under the healthy and its faulty condition is represented by means of a non-linear mapping of the corresponding feature space. Finally, a new infrared image assessment result in one diagnosis outcome for each region of interest and their

corresponding reliability index. The inference of the actual condition of the kinematic chain is carried out by means of a coherent fusion of the available information.

Such proposed diagnosis methodology provides two significant advantages: (i) the estimation of a similarity degree of the image under assessment in order to add a reliability index to the resulting diagnosis outcome and, (ii) the easiness to incorporate new fault conditions and new image segmentations to the structure.

A. Thermographic residual imaging

In order to highlight deviations over the thermal distributions in the kinematic chain, the proposed image processing stage seeks to emphasize the deviations between the thermal pattern corresponding to the healthy or nominal condition, and the thermal patterns corresponding to possible faulty conditions. In this regard, the characterization of the reference infrared images is proposed. The aim is to compute a statistical reference of the healthy thermographic representation by computing the mean of each pixel over a set of N reference infrared captures. Thus, the Reference Thermographic Image, $Ref_{TI}(x_i, y_j)$, is computed according to (3), where x_i represents the coordinate in the horizontal-axis, and y_j the coordinate in the vertical axis, with $i=1..Hr$, and $j=1..Vr$, being Hr and Vr the horizontal and vertical number of image pixels, respectively.

$$Ref_{TI}(x_i, y_j) = \sum_N^1(x_i, y_j) \quad (3)$$

Then, during the assessment of a new infrared capture, a Thermographic Residual Imaging (TRI), is obtained by direct pixel by pixel subtraction against the reference thermographic image. It is proposed also in this stage, the consideration of a smoothing 2-dimensional filter in order to improve the visualization and reduce possible outliers' affection over the resulting thermographic residual image. Such representations will show values close to zero in case of similarity with the reference condition, and values different from zero in case of dissimilarities. Hence, the differences in regard with the healthy condition will be emphasized.

B. Segmented feature extraction

Malfunctions in a kinematic chain can be, directly or indirectly, reflected in one or multiple components. Thus, an approach capable of characterize the thermal behavior of different parts is proposed. Following classical thermal image analysis procedures, the regions of interest are, first, segmented. Indeed, the segmentation of the thermographic residual images allows the possibility of a specific analysis of the kinematic chain components. This segmentation is predefined over the infrared image. Thus, segmented thermographic residual images are obtained corresponding to the components of interest, such as bearings, shafts or couplings among others. Their thermal distributions are proposed to be considered as significant source of information. The analysis of the thermal distribution corresponding to the healthy and faulty conditions of the mechanical components under monitoring would allow the root-cause identification of possible anomalies in the kinematic chain. Indeed, different anomalies may generate different affectionation patterns

distributed through the kinematic chain components. The proposed segmented feature extraction procedure is shown in Fig. 2. Dealing with thermal affectations, the proposed set of statistical numerical features to be estimated from the TRI segmentations are the mean, μ_{TRI} , (4), and the standard deviation, σ , (5). The mean represents the average value that gives some information about general brightness of the image, while the standard deviation provides information about the contrast and describes the spread in the data. In this regard, instead classical feature extraction from the totality of the segmented image, a shifting square window of predefined size w_s is proposed.

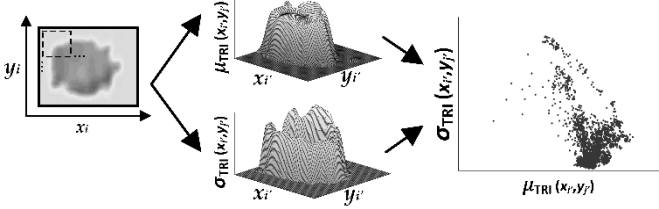


Fig. 2. Segmented feature extraction procedure. For each considered segment of the thermographic residual image, the mean, μ , and the standard deviation, σ , are estimated through a shifting windowing approach to obtain the characteristic thermal distribution under healthy and faulty conditions of the component of interest.

$$\mu_{TRI}(x_i, y_j) = \frac{\sum_{i=i^*w_s}^{i^*w_s+w_s} \sum_{j=j^*w_s}^{j^*w_s+w_s} TRI(x_i, y_j)}{w_s^2} \quad (4)$$

$$\sigma_{TRI}(x_i, y_j) = \sqrt{\frac{\sum_{i=i^*w_s}^{i^*w_s+w_s} \sum_{j=j^*w_s}^{j^*w_s+w_s} (TRI(x_i, y_j) - \bar{TRI}(x_i, y_j))^2}{w_s^2}} \quad (5)$$

C. Thermal distribution mapping

The proposed SOM structure is expected to adapt the coordinates of its matching units to the topology described in the statistical feature space of each segmented region from the thermographic residual images. The Fig. 3 illustrates the proposed SOM operation.

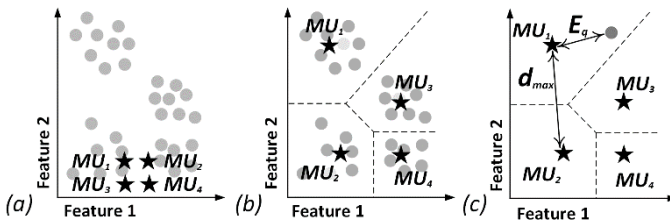


Fig. 3. Representation of the self-organizing mapping procedure in a 2-dimensional space. (a) Input data samples, \bullet , and a randomly initialized 2×2 neuron grid, \star . (b) Resulting training process. The dotted lines represent the memberships of the matching units considering Euclidian distances. The maximum distance between MU, d_{max} , corresponds to MU_1 and MU_2 . (c) New data point assessment corresponding to MU_1 activation and related E_q .

Prior to the training, the neuron grid composed by the predefined number of matching units is randomly initialized within the input data space, Fig. 3(a). During the training, Fig. 3(b), the MU's grid successively adapts the weights wn_i in order to preserve as much as possible the local topologies.

Finally, the trained grid can be evaluated with new data, Fig. 3(c), where the Euclidean distance to each MU is calculated. The nearest MU is considered the BMU and, then, activated. By this procedure, the input data can be, then, modelled by a small number of MU. Moreover, during the training process, each MU can be associated to a class label following a majority voting procedure among its nearest data points. Thus, the posterior diagnosis can be obtained.

D. Diagnosis inference

As aforementioned, the quantization error represents the distance of the data vector to its BMU. In this regard, the quantization error resulting from a new data assessment measures the amount of knowledge that the corresponding map has over such data point, that is, a similarity degree in regard with the original data used during the map training. Indeed, during the training stage, the mapping of the thermal distributions provides a mean quantization error, E_q , describing the average distance error between the data set and their corresponding BMU. Then, during the assessment stage, quantization errors, E_q , within the mean quantization error range, \bar{E}_q , represent the highest reliability degree, $R=100\%$, while E_q bigger than the distance between the two further MUs, d_{max} , represents a reliability degree $R=0\%$. The quantization error is, then, used to provide information regarding the reliability of the condition diagnosis outcome (6).

$$R = \begin{cases} E_q < \bar{E}_q, & 100 \\ E_q > [\bar{E}_q, d_{max}], & \frac{E_q}{d_{max}} - 100 \\ E_q < d_{max}, & 0 \end{cases} \quad (6)$$

IV. RESULTS

A. Experimental setup

The experimental setup used for testing the proposed methodology is shown in Fig. 4. The test bench is based on a kinematic chain driven by a variable frequency inverter, VFD, model WEGCFW08, to feed and control the rotational speed of a 1492 W, three-phase induction motor, model WEG00236ET3E145T-W22. The induction motor is coupled to a 4:1 ratio gearbox, model Baldor GCF4X01AA, driving its input shaft. Besides, the gearbox in turn couples the induction motor to a DC generator, model Baldor CDP3604, such generator is used as a non-controlled mechanical load demanding around 20% of the nominal load in the induction motor under the considered working conditions.

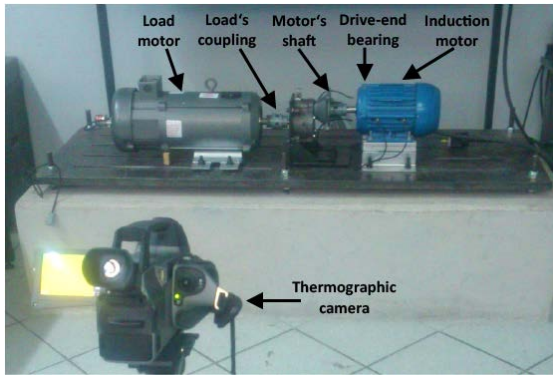


Fig. 4. Experimental test bench for the validation of the proposed thermographic data-driven methodology.

The thermal images are acquired using a thermographic camera model FLIR G320, from FLIR Systems. The camera configuration and operating conditions have been set inside the ranges recommended by the manufacturer. The environmental temperature, the relative humidity and the observation distance have been introduced to the camera for a proper image compensation. Also, by means of an initial comparison with contact temperature transducers, a value of 0.95 emissivity has been estimated and introduced. The thermal images are obtained by pseudo coloring technique [22]. Although it is possible to use different color palettes for this purpose, in this study, the gray scale has been used as suitable approach for displaying the true temperature of the objects and identify the regions that have high temperatures in reference to a background temperature. The thermographic camera takes an image of the whole kinematic chain every minute during 60 minutes once the thermal steady-state is reached. The acquired information is stored in a personal computer (PC), and analyzed in Matlab, which the proposed data-driven methodology is performed and the kinematic chain condition is obtained. From the 60 images collected for each kinematic chain condition, 40 are used during the training stage, while the remaining 20 are used for test purposes.

Four different conditions of the kinematic chain are considered during the experimental analysis. First, the Healthy condition (HLT). Second, the Bearings Defect (BD), by drilling a hole with 1.191 mm of diameter on the 6205-2ZNR bearing outer race using a tungsten drill bit as shown in Fig. 5(a). Third, the presence of Unbalance (UNB), is related to the induction motor mechanical load distribution, thus, a no uniform load distribution takes the center of mass out of the motor shaft. To do this, the UNB condition is produced by attaching a bolt in the induction motor's shaft coupling as shown in Fig. 5(b). Finally, fourth, a Misalignment (MAL) is present when the centerlines of coupled shafts do not coincide with each other, as a consequence, the dynamic load on bearings and couplings increases. Therefore, an angular misalignment is carried out by moving the free end of the induction motor, so that a misalignment of 5 mm on horizontal plane is achieved only from the free end, Fig. 5(c) shows the misalignment shaft coupling.

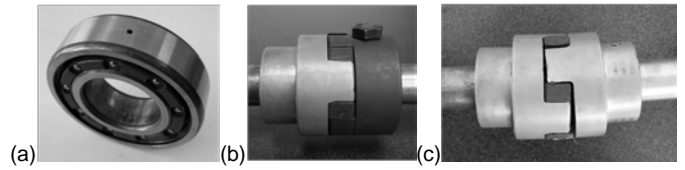
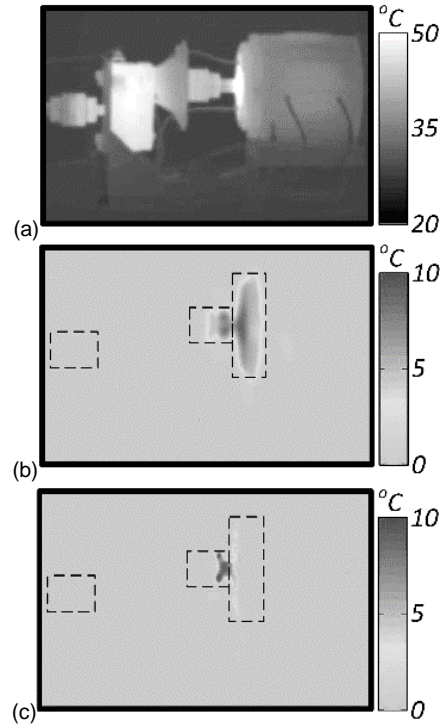


Fig. 5. Arrangement of the different faults produced in the experimental test bench. (a) Bearing defect. (b) Unbalance. (c) Misalignment.

The misalignment is considered when the coupling with the load is not properly aligned, and the unbalance occurs when the mechanical stress in the induction motor's shaft is not uniformly distributed during its rotation. In fact, the unbalance condition is considered as an eccentricity in the induction motor, which generates more mechanical stress and excessive rubbing and fatigue of the ball bearings, causing a decrease of efficiency and a rise of temperature in the induction motor [23]. In this regard, the considered bearing defect, which is a very common failure in induction motors, produces deterioration in the bearing lubrication and an abnormal friction in the bearing housing. This abnormal friction is reflected also in an increase of temperature [24], which propagates into the induction motor and other parts of the kinematic chain, increasing the risk of misclassification due to thermal patterns overlapping.

B. Competency of the method

The application of the methodology described in the previous section follows. In Fig. 5(a), an example of an infrared image in gray scale, corresponding to the healthy condition, is shown. The resulting thermographic residual images corresponding to bearing defect, unbalance and misalignment fault conditions are shown in Fig 5(b), Fig 5(c) and Fig 5(d), respectively.



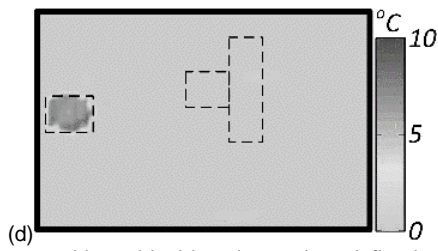


Fig. 5. Thermographic residual imaging and predefined segments. (a) Example of an original infrared thermography, healthy condition. (b) Thermographic residual image corresponding to the bearing defect fault condition. (c) Thermographic residual image corresponding to the unbalance fault condition. (d) Thermographic residual image corresponding to the misalignment fault condition.

In this application case, three components of the kinematic chain are considered for the posterior image segmentation: the drive-end’s bearing, the induction motor’s shaft, and the load’s coupling. These three regions are segmented from each computed thermographic residual image. For each of the segmented regions of interest, the thermal pattern under the healthy and its corresponding faulty condition are characterized by means of the statistical-time features estimation for training purposes. Thus, first, from the drive-end’s bearing segment, the healthy and the bearing defect conditions are characterized. Second, from the motor’s shaft region, the healthy and unbalance conditions are characterized. Finally, third, from the load’s coupling region, the healthy and the misalignment conditions are characterized. The resulting 2-dimensional statistical feature spaces for the drive-end’s bearing region, the motor’s shaft region and the load’s coupling region under the healthy and its corresponding faulty condition are shown in Fig. 6(a), Fig. 7(a) and Fig 8(a), respectively.

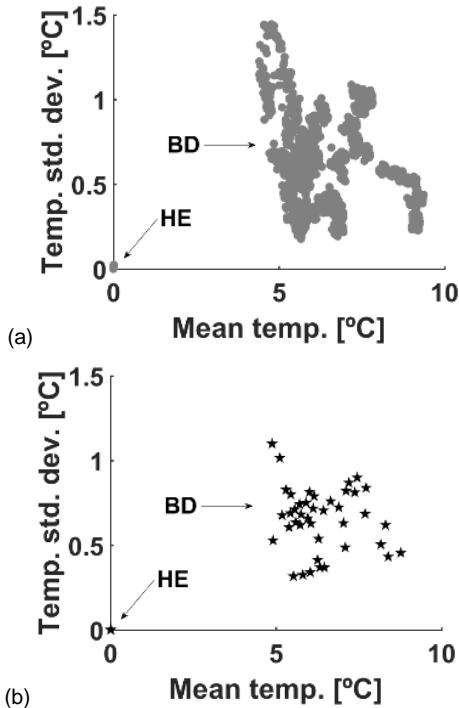


Fig. 6. Thermal distribution of the drive-end’s bearing region under healthy and bearing defect conditions. (a) Statistical features characterization, ●. (b) Resulting self-organizing map, ★.

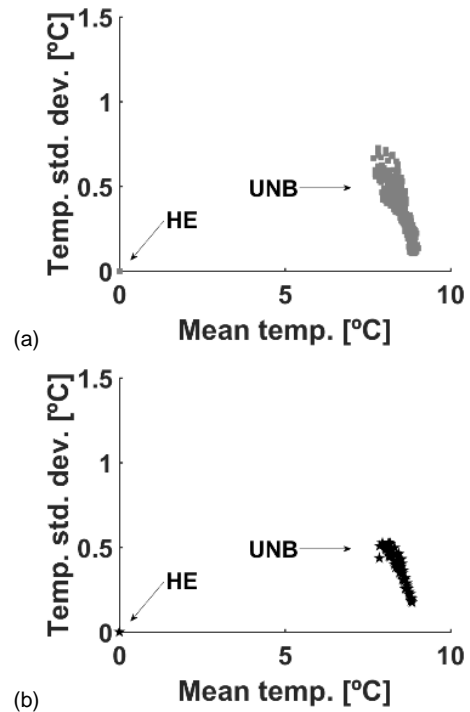


Fig. 7. Thermal distribution of the motor’s shaft region under healthy and unbalance conditions. (a) Statistical features characterization, ●. (b) Resulting self-organizing map, ★.

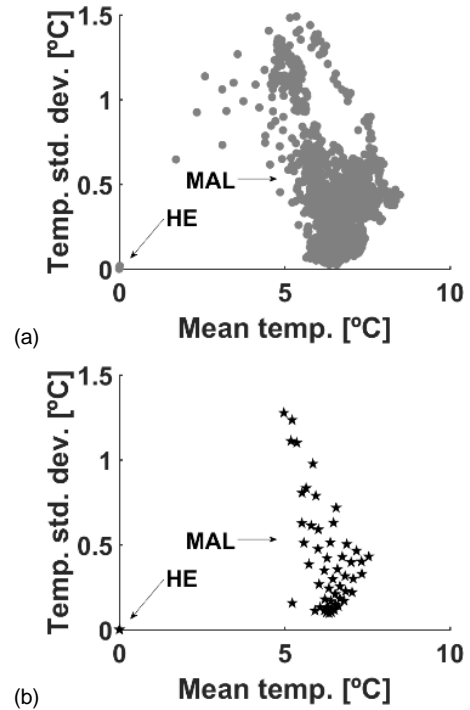


Fig. 8. Thermal distribution of the load’s coupling region under healthy and misalignment conditions. (a) Statistical features characterization, ●. (b) Resulting self-organizing map, ★.

The thermal distributions resulting from the healthy condition of the kinematic chain analyzed from the three considered regions lead to the computation of the reference thermographic image. In regard with the fault conditions, it must be noted that, although no information about the geometry of the component under monitoring is directly kept,

the resulting thermal distributions are distinctive for each fault condition as well as its thermal affectation over the mechanical element considered in the corresponding segmented region. Thus, although the three fault conditions exhibit generalized temperatures increases, between 5 - 10°C in terms of mean temperature, and between 0.5 - 1.5°C in terms of deviation over the mean, the characteristic fault thermal patterns are different.

Next, the mapping of such thermal distributions is carried out. In this regard, a 10-by-10 neuron grid is used as a simple SOM structure for the mapping of each of the statistical feature spaces resulting from the three region of interest. The resulting maps corresponding to the drive-end's bearing region, the motor's shaft region, and the load's coupling region under the healthy and their corresponding faulty condition are shown in Fig. 6(b), Fig. 7(b) and Fig 8(b), respectively. As aforementioned, this thermal distribution mapping stage has been carried out to characterize the thermal distributions of the component under monitoring over the healthy and corresponding faulty condition. In consequence, the three resulting maps will provide binary diagnosis condition outcomes between: healthy/bearing defect, healthy/unbalance and healthy/misalignment. A visual inspection of the resulting self-organized maps reveals their suitability in regard with the corresponding feature spaces. Quantitatively, the resulting quantization mean error, \bar{E}_q , for each map, reinforces the aforementioned since all of them are very low: 0.077 for the drive-end's bearing feature space, 0.010 for the motor's shaft feature space, and 0.049 for the load's coupling feature space.

The validation of the thermal distribution mapping has been carried out by means of a test set of infrared images corresponding to the healthy and three fault conditions. Thus, first, in regard with the drive-end's bearing region, its thermal affectation pattern in front of healthy, bearing defect, unbalance and misalignment conditions is shown in Fig 9. As expected, the healthy condition affectation exhibits no significant deviations regarding the reference thermographic image. Similarly, the thermal effects of the misalignment fault condition does not affect the drive-end's bearings, which is a coherent behavior considering the mechanical structure of the kinematic chain. The thermal affectation under the bearing defect condition match, as expected, with the corresponding mapped distribution. However, the unbalance fault condition produces a significant variation of temperature in regard with the healthy condition. It is interesting to observe that the unbalance fault condition slightly affects the end-drive's bearing region.

Second, in regard with the induction motor's shaft region, the resulting thermal patterns are shown in Fig. 10. The healthy condition, as well as the misalignment fault condition, do not reveal significant deviations over the nominal thermal behavior. In this case, the unbalance fault condition, as expected, match significantly with the corresponding mapped distribution. However, the bearing defect fault condition shows an affectation over the expected nominal thermal distribution in the motor's shaft.

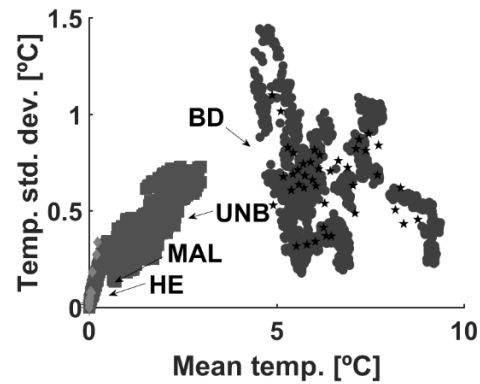


Fig. 9. Projection of the four data sets into the drive-end's bearing self-organizing map, ★: healthy condition, * , misalignment fault, ◆ , unbalance fault, ■ , and bearing defect fault, ● .

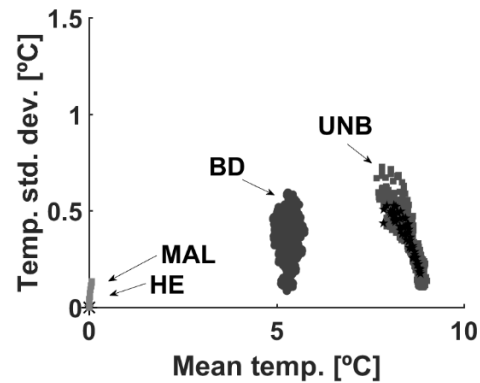


Fig. 10. Projection of the four data sets into the motor's shaft self-organizing map, ★: healthy condition, * , misalignment fault, ◆ , unbalance fault, ■ , and bearing defect fault, ● .

Finally, third, in regard with the load's coupling region, as it can be seen in Fig. 11, the healthy, as well as the bearing defect and unbalance fault conditions show no thermal affectations, while the misalignment fault condition, as expected, exhibits a clear match with the corresponding mapped distribution.

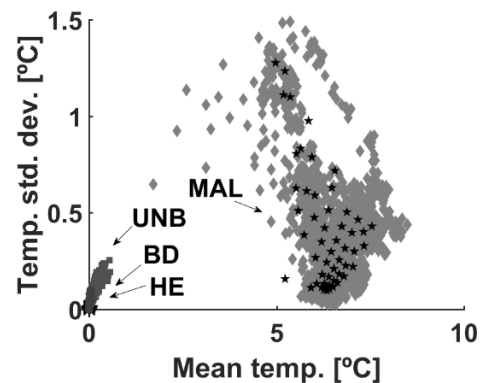


Fig. 11. Projection of the four data sets into the load's coupling self-organizing map, ★: healthy condition, * , misalignment fault, ◆ , unbalance fault, ■ , and bearing defect fault, ● .

Indeed, the assessment of each of the infrared images through the proposed methodology provides, a part of the 2-dimensional visualizations, three condition diagnosis outcomes and its corresponding reliability indexes, one pair per considered region of interest. Hence, a pair of diagnosis outcome and a reliability index is obtained from the drive-end's bearing, from the motor's shaft, and, also, from the

load’s coupling regions of interest, as shown in Fig. 12, Fig. 13 and Fig. 14, respectively. Thus, in Fig 12(a), Fig 13(a) and Fig. 14(a), the resulting condition diagnosis between HLT and BD, HLT and UNB, and HLT and MAL, respectively, in front of all conditions considered is shown. In Fig 12(b), Fig 13(b) and Fig. 14(b), the corresponding reliability indexes of each diagnosis outcome are shown, where 100% of reliability means, as depicted in (6), a totally reliable diagnosis outcome.

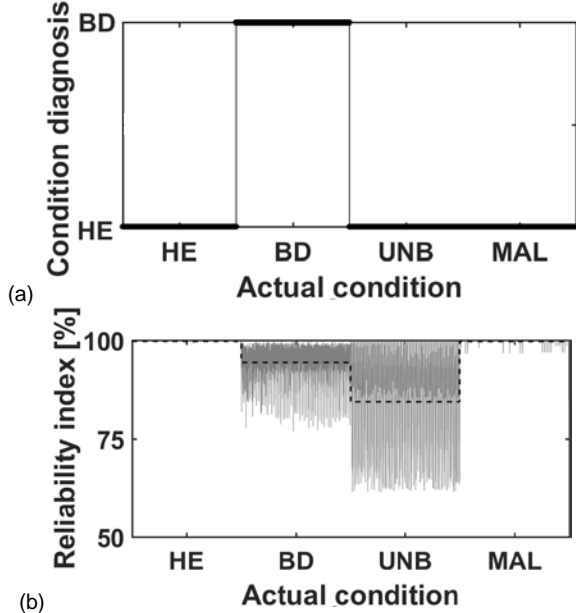


Fig. 12. Diagnosis results from the drive-end’s bearing region of interest in front of the four data sets: healthy (HE), bearing defect (BD), unbalance (UNB), and misalignment (MAL). (a) Condition diagnosis results, •. (b) Reliability indexes, per sample, -, and averaged, - -.

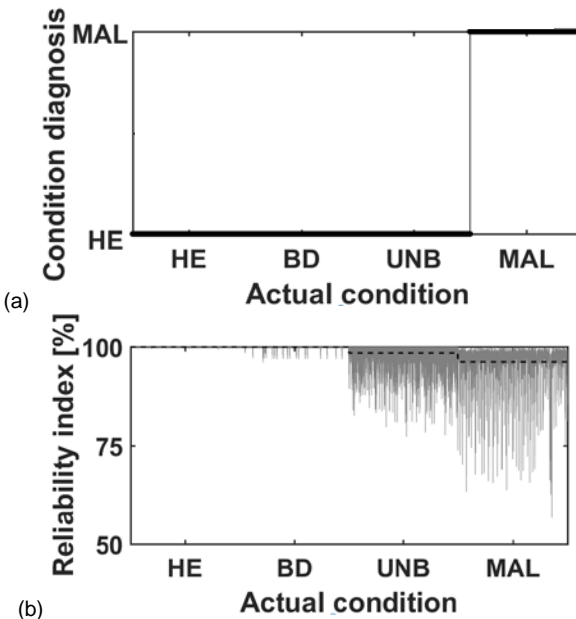


Fig. 13. Diagnosis results from the motor’s shaft region of interest in front of the four data sets: healthy (HE), bearing defect (BD), unbalance (UNB), and misalignment (MAL). Condition diagnosis results, •, and reliability indexes, per sample, -, and averaged, - -.

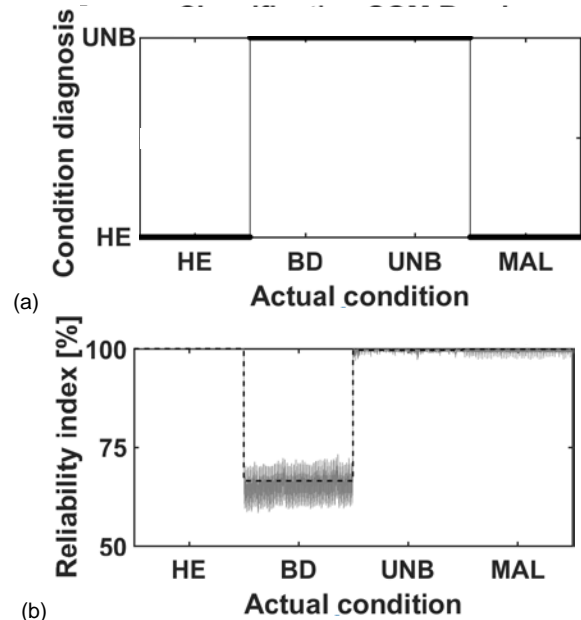


Fig. 14. Diagnosis results from the load’s coupling region of interest in front of the four data sets: healthy (HE), bearing defect (BD), unbalance (UNB), and misalignment (MAL). Condition diagnosis results, •, and reliability indexes, per sample, -, and averaged, - -.

As shown in Table I, the kinematic chain condition and the actual root-cause malfunction is inferred through the fusion of all three diagnosis outcomes and corresponding reliability indexes. It is important to notice that, although the unbalance fault condition has been diagnosed as healthy from the drive-end’s bearing region, the reliability associated to such diagnosis is around the 80%, while the condition diagnosis as unbalance fault from the induction motor’s shaft region reaches a 99.6% of reliability. Similar effect is detected when the bearing defect fault conditions is analyzed. From the drive-end’s bearing region, the reliability of the diagnosis reaches 99.7%, while from the induction motor’s shaft region fall below 70%. That is, although different faults can affect thermally multiple components in the kinematic chain, this affection results in different thermal distributions depending on the actual root-cause, which is quantified in the proposed methodology by the reliability index estimation.

TABLE I
THERMOGRAPHIC DATA-DRIVEN METHODOLOGY TEST RESULTS
DIAGNOSIS OUTCOME | RELIABILITY INDEX [%]

Region	Induction motor’s shaft	Load’s coupling	Drive-end bearing
Actual condition			
Healthy	HE 99.9	HE 99.95	HE 99.7
Unbalance	UNB 99.6	HE 98.5	HE 84.4
Misalignment	HE 99.8	MAL 96.2	HE 99.7
Bearing	UNB 66.5	HE 99.9	BD 94.3

In this sense, the presence of fault conditions in the resulting set of diagnosis outcomes prevail over the healthy conditions since the detection of a temperature increase represents an explicit effect of malfunction. In this regard, the healthy condition of the kinematic chain can be only considered by unanimity of all the diagnosis outcomes. The reliability index, then, provides information about thermal

deviations degrees beyond the fault detection. The reliability index allows the quantization of the possible thermal deviation of the kinematic chain and, even, the identification of the most affected component under monitoring, which allows the inference of the actual malfunction root-cause.

Indeed, such root-cause identification capabilities provided by the proposed method represents a significant advance compared with classical temperature gradient analyses. In this regard, dealing with the same experimental setup and infrared images sets, the classical maximum temperature gradient method [25], has been applied. As shown in Table II the method exhibits important limitations.

TABLE II
CLASSICAL MAXIMUM TEMPERATURE GRADIENT METHOD TEST RESULTS
MAXIMUM TEMPERATURE GRADIENT [°C]

Actual condition \ Region	Induction motor's shaft	Load's coupling	Drive-end bearing
Healthy	0	0	0
Unbalance	9.1	0	3.7
Misalignment	0	8.8	0
Bearing	6.2	0	9.3

Thus, although the misalignment fault condition can be detected and identified, the bearing defect and unbalance fault conditions lead to a non-conclusive diagnosis, limiting the approach to a fault detection scheme. In this regard, the thermal distribution consideration together with the reliability index provided by the proposed method is revealed as an enhanced diagnosis approach.

V. CONCLUSIONS

This paper presents a novel methodology based on thermographic data-driven for multi-fault diagnosis on kinematic chains. There are three important aspects in this new method. The first one is the thermographic residual image representation. The computation of a statistical reference of the kinematic representation allows to emphasize the thermal affectation of possible faults. Such approach enhances the fault patterns characterization but, moreover, represents an interesting strategy to identify deviations from the nominal behavior. Indeed, the industrial applicability of the proposed method is possible since only the nominal behavior is initially required. In this regard, the diagnosis capabilities would evolve from fault detection to fault identification as more conditions become available and incorporated to the method. The second is the application of a segmented statistical feature extraction. The segmentation of the thermographic images is a usual solution to focus the analysis on specific components in the electromechanical system. However, despite classical approaches based on maximum temperature gradient value, the proposed methodology proposes the characterization of the thermal distribution by statistical features. Indeed, although the classical temperature increase quantification represents a significant sign of malfunction, the characterization of the thermal distribution for each kinematic chain component

under inspection represents a higher resolution method in order to allow the identification of the actual root-cause. The proposed set of statistical features allows a 2-dimensional visualization of the fault appearance but, also, the affectation degree of the fault to the component under analysis. The third is the use of a thermal distribution modelling for classification based on self-organizing maps. The neural network grids are used to map the thermal distributions preserving, as much as possible, the topological properties of the data. The proposed thermal mapping allows the diagnosis of the kinematic chain condition and, complementary, provides information about the reliability of such assessment, which allow to infer the diagnosis and the identification of the actual root-cause of malfunction. Four different experimental conditions have been considered, which represents an important range of system conditions, including healthy and three faulty scenarios. Under all of these experimental conditions, the proposed methodology shows enhanced diagnosis results compared with the classical methods. The results obtained in this work suggest that this methodology may be also useful for any other rotating mechanical component faults, diagnosing certain failures and complementing the diagnosis conclusions reached with other physical magnitudes to reduce eventual false alarms. Future work will focus in the analysis of multi-fault diagnosis methodology considering fault severities and different operating conditions of speed and load.

REFERENCES

- [1] L. Frosini, C. Harlişca and L. Szabó, "Induction Machine Bearing Fault Detection by Means of Statistical Processing of the Stray Flux Measurement," *IEEE Trans. Ind. Electron.*, vol. 62, no. 3, pp. 1846-1854, Mar. 2015.
- [2] O. Janssens, V. Slavkovikj, B. Vervisch, K. Stockman, M. Loccufier, S. Verstockt, R. Van de Walle and S. Van Hoecke, "Convolutional Neural Network Based Fault Detection for Rotating Machinery," *J. Sound Vib.*, vol. 377, pp. 331-345, Sep. 2016.
- [3] J. Lee, F. Wu, W. Zhao, M. Ghaffari, L. Liao, and D. Siegel, "Prognostics and health management design for rotary machinery systems - Reviews, methodology and applications," *Mech. Syst. Signal Process.*, vol. 42, no. 1-2, pp. 314-334, Jan. 2014.
- [4] M. Drif and A. J. M. Cardoso, "Stator Fault Diagnostics in Squirrel Cage Three-Phase Induction Motor Drives Using the Instantaneous Active and Reactive Power Signature Analyses," *IEEE Trans. Ind. Inform.*, vol. 10, no. 2, pp. 1348-1360, May 2014.
- [5] J. J. Saucedo-Dorantes, M. Delgado-Prieto, J. A. Ortega-Redondo, R. A. Osornio-Rios and R. J. Romero-Troncoso, "Multiple-Fault Detection Methodology Based on Vibration and Current Analysis Applied to Bearings in Induction Motors and Gearboxes on the Kinematic Chain," *Shock and Vibration*, vol. 2016, pp. 1-13, Feb. 2016.
- [6] M. Suguna, S. M. M. Roomi and I. Sanofer, "Fault localisation of electrical equipments using thermal imaging technique," in *Proc. Inter. Conf. on Emerging Technological Trends (ICETT)*, Kerala, India, Oct. 2016.
- [7] M. J. Picazo-Ródenas, J. Antonino-Daviu, V. Climente-Alarcon, R. RoyoPastor, and A. Mota-Villar, "Combination of Noninvasive Approaches for General Assessment of Induction Motors," *IEEE Trans. Ind. Appl.*, vol. 51, no. 3, pp. 2172-2180, Jun. 2015.
- [8] W. Pawlus, H. Van Khang and M. Rygaard Hansen, "Temperature Rise Estimation of Induction Motor Drives Based on Loadability Curves to Facilitate Design of Electric Powertrains," *IEEE Trans. Ind. Inform.*, vol. 13, no. 3, pp. 985-994, Jun. 2017.
- [9] M. Shawal and S. Taib, "Infrared Physics & Technology Recent progress in diagnosing the reliability of electrical equipment by using infrared thermography," *Infrared Phys. Technol.*, vol. 55, no. 4, pp. 236-245, Jul. 2012.

- [10] P. Gill, *Electrical Power Equipment Maintenance and Testing*, Boca Raton, FL, USA: CRC Press, 2009.
- [11] S. B. Lee, E. Wiedenbrug, and K. Younsi, "ECCE 2013 tutorial: testing and diagnostics of induction machines in an industrial environment," in *Proc. IEEE Energy Convers. Congr. Expo.*, Colorado, Denver, USA, Sep. 2013.
- [12] D. López-Pérez and J. Antonino-Daviu, "Application of Infrared Thermography to Failure Detection in Industrial Induction Motors: Case Studies," *IEEE Trans. Ind. Appl.*, vol. 53, no. 3, pp. 1901-1908, Jun. 2017.
- [13] M.J. Picazo-Ródenas, R. Royo, J. Antonino-Daviu, and J. Roger-Folch, "Use of the infrared data for heating curve computation in induction motors: Application to fault diagnosis," *Engineering Failure Analysis*, vol. 35, pp. 178-192, Dec. 2013.
- [14] A. Younus and B. Yang, "Intelligent fault diagnosis of rotating machinery using infrared thermal image," *Expert. Syst. Appl.*, vol. 39, no. 2, pp. 2082-2091, Feb. 2012.
- [15] P. Karvelis, G. Georgoulas, C. D. Stylios, J. A. Antonino-daviu, and M. J. Picazo, "An Automated Thermographic Image Segmentation Method for Induction Motor Fault Diagnosis," in *Proc. IEEE Ind. Electron. Soc. Conf.*, Dallas, Texas, USA, Nov. 2014, pp. 3396-3402.
- [16] A. G. Garcia-Ramirez, L. Alberto Morales-Hernandez, R. A. Osornio-Rios, J. P. Benitez-Rangel, A. Garcia-Perez, and R. de J. Romero-Troncoso, "Fault detection in induction motors and the impact on the kinematic chain through thermographic analysis," *Electric Power Systems Research*, vol. 114, pp. 1-9, Sep. 2014.
- [17] V. Tung Tran, B.-S. Yang, F. Gu, and A. Ball, "Thermal image enhancement using bi-dimensional empirical mode decomposition in combination with relevance vector machine for rotating machinery fault diagnosis," *Mechanical Syst. Signal Processing*, vol. 38, no. 2, pp. 601-614, Jul. 2013.
- [18] S. D. Villalba and P. Cunningham, "An evaluation of dimension reduction techniques for one-class classification," *Artif. Intell. Rev.*, vol. 27, no. 4, pp. 273-294, Apr. 2007.
- [19] Z. Zhang, J. Wang, and H. Zha, "Adaptive Manifold Learning," *IEEE Trans. Pattern Anal. Mach. Intell.*, vol. 34, no. 2, pp. 253-265, Feb. 2012.
- [20] R. N. Wurzbach, and R. G. Hammaker, "Role of comparative and qualitative thermography in predictive maintenance," in *Proc. Intl Conf on Thermal Sensing and Imaging Diagnostic Applications*, Apr. 1992, vol. 1682, pp. 3-11.
- [21] *Standard for Infrared Inspection of Electrical Systems & Rotating Equipment*, Infrasppection Institute, Burlington, NJ, USA, 2008.
- [22] R. Jayadevan, K.N. Latha, K.A. Navas, and Anjali. Ananthan, "A Review on Recent Pseudo-Coloring Techniques", *Int. J. Sci. Tech. Eng.*, vol. 1, no. 11, pp. 344-348, Jun. 2015.
- [23] Y. Zhou, X. Bao, C. Di, and L. Wang, "Analysis of dynamic unbalanced magnetic pull in induction motor with dynamic eccentricity during starting period," *IEEE Trans. Magn.*, vol. 52, no. 7, Jun. 2016.
- [24] C. Zhang and S. Wang, "Experimental analysis of performance degradation of solid lubricated bearings with vibration and friction torque signal," in *Proc. IEEE Int. Conf. on Ind. Inf.*, Beijing, pp. 617-620, Jul. 2012.
- [25] O. Munoz-Ornelas, D. A. Elvira-Ortiz, R. A. Osornio-Rios, R. J. Romero-Troncoso and L. A. Morales-Hernandez, "Methodology for thermal analysis of induction motors with infrared thermography considering camera location," in *Proc. IEEE Ind. Electron. Soc.*, Oct. 2016, pp. 7113-7118.